

Calculation of Ligand Dissociation Energies in Large Transition-Metal Complexes

Tamara Husch, Leon Freitag, and Markus Reiher*

ETH Zürich, Laboratorium für Physikalische Chemie,
Vladimir-Prelog-Weg 2, 8093 Zürich, Switzerland.

March 22, 2018

Abstract

The accurate calculation of ligand dissociation (or equivalently, ligand binding) energies is crucial for computational coordination chemistry. Despite its importance, obtaining accurate *ab initio* reference data is difficult and density-functional methods of uncertain reliability are chosen for feasibility reasons. Here, we consider advanced coupled-cluster and multi-configurational approaches to reinvestigate our WCCR10 set of ten gas-phase ligand dissociation energies [J. Chem. Theory Comput. 10 (2014) 3092]. We assess the potential multi-configurational character of all molecules involved in these reactions with a multi-reference diagnostic [Mol. Phys. 115 (2017) 2110] in order to determine where single-reference coupled-cluster approaches can be applied. For some reactions of the WCCR10 set, large deviations from density-functional results including semiclassical dispersion corrections from experimental reference data had been observed. This puzzling observation deserves special attention here and we tackle the issue (i) by comparing to *ab initio* data that comprise dispersion effects on a rigorous first-principles footing and (ii) by a comparison of density-functional approaches that model dispersion interactions in various ways. For two reactions, species exhibiting nonnegligible static electron correlation were identified. These two reactions represent hard problems for electronic structure methods, also for multi-reference perturbation theories. However,

*corresponding author: markus.reiher@phys.chem.ethz.ch; Phone: +41446334308; Fax: +41446321021.

most of the ligand dissociation reactions in WCCR10 do not exhibit static electron correlation effects, and hence, we may choose standard single-reference coupled-cluster approaches to compare with density-functional methods. For WCCR10, the Minnesota M06-L functional yielded the smallest mean absolute deviation of 13.2 kJ mol^{-1} out of all density functionals considered (PBE, BP86, BLYP, TPSS, M06-L, PBE0, B3LYP, TPSSh, and M06-2X) without additional dispersion corrections in comparison to the coupled-cluster results and the PBE0-D3 functional produced the overall smallest mean absolute deviation of 4.3 kJ mol^{-1} . The agreement of density-functional results with coupled-cluster data increases significantly upon inclusion of any type of dispersion correction. It is important to emphasize that different density-functional schemes available for this purpose perform equally well. The coupled-cluster dissociation energies, however, deviate from experimental results on average by 30.3 kJ mol^{-1} . Possible reasons for these deviations are discussed.

1 Introduction

A detailed assessment of approximate density functionals is crucial for drawing meaningful conclusions from quantum chemical studies of transition-metal complexes and their reactions.¹⁻¹¹ One of the few benchmark sets for large transition-metal complexes containing experimental gas-phase reference data is our WCCR10 reference set of ligand bonding energies.¹²

The WCCR10 set comprises ten experimentally measured gas-phase ligand dissociation energies obtained from threshold collision-induced decay (T-CID) experiments. For nine density functionals, we found mean absolute errors larger than 26.7 kJ mol^{-1} with largest absolute errors as large as 83.4 kJ mol^{-1} for the WCCR10 energies.¹² For most of the ligand dissociation energies, the subsequent inclusion of semiclassical dispersion corrections yielded¹² results which deviated even further from the experimental results although they should have brought the results in closer agreement with the experimental data; the reason for this has remained unclear. In a subsequent study,¹³ we attempted to reparametrize the standard BP86¹⁴ functional to achieve better agreement with the experimental reference energies. We found,¹³ however, that this goal cannot be achieved with a single parameter set. So far, results obtained with a new functional reported by the Truhlar group (MN15-L) agreed best with the experimental WCCR10 data (mean absolute deviation of 22.8 kJ mol^{-1}).¹⁵

Further studies attempted to elucidate the poor performance of density functional theory (DFT). Kobylanskii *et al.*¹⁶ found large discrepan-

cies between calculated and measured Co–C dissociation energies in two organocobalamins. Qu *et al.*¹⁷ studied the discrepancies for these cobalamines in more detail and claimed that the procedure with which the dissociation energies are extracted from T-CID experiments cannot be rigorously validated for molecules larger than 50 atoms and the discrepancy might not be a failure of the theoretical description. Pollice *et al.*¹⁸ attempted to address this issue partially in a later paper, but the discrepancies persisted.

Evidently, the description of the electronic structure of large transition-metal complexes is still a challenging task because electronic structures of multi-configurational character may be encountered. For single-configurational cases, coupled-cluster (CC) methods at the basis-set limit turned out to be very reliable.^{19–25} Recent developments such as the domain-based local pair-natural-orbital CC (DLPNO-CC) approach of the Neese group^{26,27} or the pair-natural-orbital local CC (PNO-CC) approach of the Werner group²⁸ with explicit correlation factors (PNO-LCCSD-F12)²⁹ make CC calculations feasible for large molecules. Single-reference CC theory is, however, generally not applicable for molecules which exhibit strong static electron correlation. Unfortunately, decades of research on multi-reference CC theories (see, for instance, Refs. 30–35) have not led to a unique model that is as well-defined and efficient as its single-reference analogs are. Consequently, multi-reference perturbation theories, which require a distinction between static and dynamic electron correlation, are still a very good option in cases of strong electron correlation. Static electron correlation is then captured with a complete active space self-consistent field (CASSCF) ansatz^{36,37} which requires the selection of a limited number of active orbitals. This selection, however, can be achieved in a fully automated fashion.^{38–40} The density matrix renormalization group (DMRG)^{41–56} ansatz provides access to much larger active orbital spaces than those that are in reach for the standard CASSCF approaches. The dynamical electron correlation is quantified afterwards by multi-reference perturbation theory, such as second-order CAS perturbation theory (CASPT2)^{57,58} and N -electron valence perturbation theory to second-order (NEVPT2).^{59–61} CASPT2 and NEVPT2 calculations have become feasible for large transition-metal molecules, e.g., through Cholesky decomposition (CD) of the two-electron integrals,^{62–65} through the application of density-fitting approaches,⁶⁶ and through the development of methods applying localized molecular orbitals.^{67–70} In general, the efficient implementation of multi-reference perturbation theories that can deal with the large active spaces accessible through DMRG has been the subject of intense research in the past decade.^{65,71–78}

Here, we investigate the multi-configurational character and the role of static electron correlation in the WCCR10 set based on DMRG calculations.

In particular, we discuss the suitability of single-reference approaches and then consider DLPNO-CCSD(T) ligand dissociation energies. Very recently, Ma *et al.*²⁹ presented PNO-LCCSD-F12 WCCR10 ligand dissociation energies, to which we compare our DLPNO-CCSD results. We then re-assess several density functionals with a focus on dispersion interactions with reference to DLPNO-CCSD(T).

2 Computational Methodology

We adopted BP86^{14,79}/def2-QZVPP⁸⁰ and BP86-D3(0)⁸¹/def2-QZVPP optimized structures of all compounds in this work from Ref. 12 to facilitate a direct comparison with our previous work and with recent results published by Ma *et al.*^{29,82} The molecular structures employed in the multi-configurational calculations were the same as those in the single-configurational calculations. However, for the calculation of the dissociated complex, unlike in the single-configurational calculations, the two fragment structures were merged into one structure file with the two fragments separated by 10 Å to facilitate the selection of the active orbital space. The ground state for all molecules involved in reactions of the WCCR10 set is the closed-shell singlet state. We did not find any lower-lying open-shell singlet states when calculating the singlet states as unrestricted singlets. The triplet states are unanimously higher in energy than the singlet states (see also Table 16 in the Supporting Information)

We carried out second-order Møller–Plesset (MP2) perturbation-theory, spin-component-scaled (SCS-)MP2,⁸³ and DLPNO-CCSD(T)²⁶ coupled-cluster calculations with the ORCA program (version 4.0.1).⁸⁴ The frozen-core approximation was invoked for all wave-function-based calculations. In all MP2 calculations, we exploited resolution-of-the-identity (RI) density fitting. Auxiliary cc-pVTZ/C or cc-pVQZ/C bases⁸⁵ were specified for the RI density fitting in the MP2 calculations. We denote single-point energies determined with a given method as a first entry in front of a double slash followed by a second entry for the method employed in the molecular structure optimization, e.g., DLPNO-CCSD(T)//BP86. For all MP2, SCS-MP2, and DLPNO-CCSD(T) calculations, we chose a cc-pVTZ or a cc-pVQZ basis set⁸⁶ for all main group elements and a cc-pVTZ-PP or a cc-pVQZ-PP basis set^{87–89} for all transition metals. Stuttgart effective core potentials^{87–89} substituted the relativistic core electrons of all transition-metal atoms. From the energies obtained with the cc-pVTZ(-PP) basis set and the energies obtained with the cc-pVQZ(-PP) basis set, we extrapolated to energies at the complete basis set (CBS) limit as proposed in Ref. 90 (see also the Supporting Infor-

mation). We only discuss DLPNO-CCSD(T)/CBS energies in the main text. All underlying Hartree-Fock calculations were accelerated by the RIJCOSX⁹¹ approximation with a corresponding Coulomb fitting basis.⁹² All single-point energies were converged to 10^{-8} Hartree (ORCA keyword `TightSCF`). We verified the stability of the self-consistently obtained Hartree-Fock solutions by drastically perturbing the molecular orbitals as described in Ref.⁹³ The results presented in the main text were obtained with `NormalPNO` thresholds as recommended in Ref. 94.

We calculated single-point energies with ORCA with several popular density functionals: BLYP,^{79,95} BP86, PBE,^{96,97} M06-L,⁹⁸ TPSS,⁹⁹ B3LYP,^{95,100} PBE0,¹⁰¹ M06-2X,⁹⁸ and TPSSh,^{102,103} all with a def2-QZVPP basis set⁸⁰ and with a def2-ecp effective core potential¹⁰⁴ for Pt, Ru, Au, Ag, and Pd (all other metals were considered in all-electron calculations). For all pure functionals, the RI approximation was applied (def2/J fitting basis⁹²). In calculations involving hybrid functionals, the RIJCOSX⁹¹ approximation was activated.

All D3 dispersion (including Axilrod-Teller-Muto contributions⁸¹) were calculated with the stand-alone DFT-D3 program¹⁰⁵ of Grimme and collaborators. We applied the Becke-Johnson damping function for calculating the D3 dispersion contributions for BLYP, BP86, PBE, TPSS, B3LYP, PBE0, and TPSSh and the zero-damping function for M06-L and M06-2X as recommended in Ref. 106. We abbreviate the semiclassical D3 dispersion corrections with a zero damping function as D3(0) and the one with a Becke-Johnson damping function as D3(BJ).¹⁰⁷

We considered other types of dispersion corrections in the context of B3LYP calculations: We chose a nonlocal (NL) van-der-Waals functional which was adapted from VV10¹⁰⁸ for the B3LYP exchange-correlation functional.¹⁰⁹ The single-point energies with this functional were evaluated with ORCA and the dispersion correction was obtained both self-consistently (B3LYP-SCNL) and non-self-consistently (B3LYP-NL). We also calculated dispersion corrections with the density-dependent exchange-hole dipole moment (XDM) model.¹¹⁰⁻¹¹⁵ The required B3LYP/def2-QZVPP electron densities were obtained with the GAUSSIAN program¹¹⁶ and post-processed with the stand-alone POSTG program.¹¹⁷ The XDM calculations involve two empirical parameters which were set to $a_1 = 0.6356$ and $a_2 = 1.5119$, as recommended for a near-complete basis set.¹¹⁷

We carried out multi-reference CASPT2 calculations. The IPEA shift¹¹⁸ was set to zero in the CASPT2 calculations to facilitate comparison with single-reference MP2 results. To estimate the basis-set effect and deviations from single-reference MP2 calculations, we also calculated MP2 dissociation energies in the ANO-RCC basis set. Moreover, we carried out *self-consistent-*

field DMRG with subsequent strongly contracted NEVPT2 (SC-NEVPT2). We denote these calculations as DMRG-SC-NEVPT2; note that we omit the "SCF" label for the sake of brevity in this notation. Accordingly, we denote partially contracted (PC) calculations as DMRG-PC-NEVPT2.

We applied our automated orbital selection protocol³⁸⁻⁴⁰ for multi-configurational calculations combined with a multi-configurational diagnostic,¹¹⁹ $Z_{s(1)}$, calculated from single-orbital entropies^{120,121} that were extracted from a qualitatively correct multi-configurational wave function. The $Z_{s(1)}$ multi-configurational diagnostic¹¹⁹ was calculated from the automatically selected active space, unless noted otherwise. Due to the very low multi-configurational character of some compounds and the necessity to have consistent active orbital spaces for the undissociated complex and its fragments, we adjusted the final orbital selection. Details on the active-space selection procedure are provided in the Supporting Information.

We chose the all-electron ANO-RCC¹²² basis set with the valence quadruple-zeta polarized (ANO-RCC-VQZP) contraction scheme for the metal atoms and the valence triple-zeta polarized (ANO-RCC-VTZP) contraction scheme for other atoms. For reaction 4, where multi-reference perturbation theory with this basis set would be computationally unfeasible, and hence, a valence double-zeta polarized (ANO-RCC-VDZP) basis set was chosen. This mixed basis set is denoted "ANO-RCC" for simplicity in the following. Two-electron integrals were calculated with the atomic compact Cholesky decomposition (CD) approach^{63,123,124} with a decomposition threshold of 10^{-4} . Scalar-relativistic effects were accounted for through the second-order scalar-relativistic Douglas-Kroll-Hess one-electron Hamiltonian.¹²⁵⁻¹²⁷ All calculations were performed with a locally modified version of OPENMOLCAS.¹²⁸ For the self-consistent-field DMRG and DMRG-NEVPT2 calculations, we chose our implementations QCMAQUIS¹²⁹⁻¹³² and CD-NEVPT2,⁶⁵ which are both interfaced to OPENMOLCAS. The number of renormalized block states m for all DMRG calculations was chosen such that the truncation error of the DMRG wave function was less than 10^{-7} a. u., which corresponds to $m=2048$ for reaction 9 and $m=1024$ for all other reactions.

For reaction 10, an active space of 17 orbitals was automatically selected which is, however, too large for a CASPT2 calculation for molecules of this size. Therefore, we manually selected a smaller active orbital space comprising only nine orbitals for this reaction. We carried out DMRG-SC-NEVPT2 calculations with the full (17 orbitals) and reduced (9 orbitals) active orbital spaces which resulted in ligand dissociation energies that differed by only 1.8 kJ mol⁻¹. We consequently chose this reduced active space for reaction 10 for all multi-configurational calculations in this work.

3 WCCR10 Set of Coordination Energies

The WCCR10 data set¹² contains ten experimentally determined ligand dissociation energies of large transition-metal complexes (Figure 1). These cationic complexes feature different transition metals (Au, Ag, Pt, Ru, Cu, Pd) and a diverse selection of ligand environments.

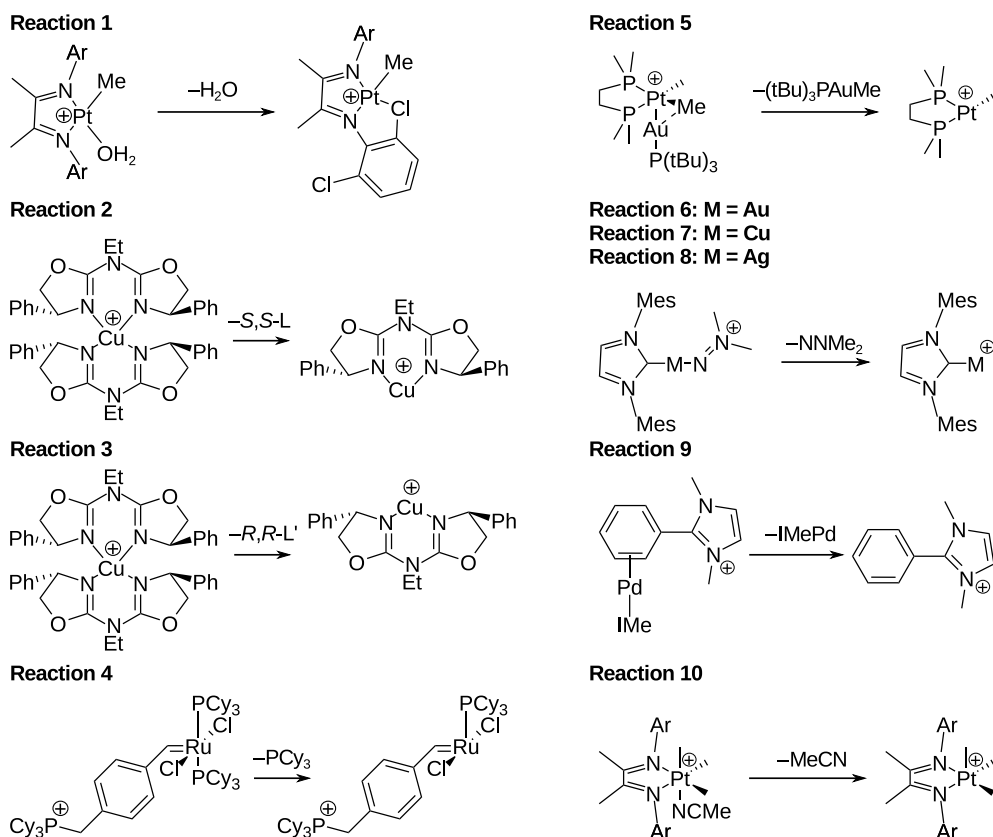


Figure 1: Overview of the ten ligand dissociation reactions in the WCCR10 set. The abbreviation "Ar" denotes a 2,6-C₆H₃Cl₂ substituent. The abbreviations "S,S-L" and "R,R-L'" refer to the neutral ligands (L and L') dissociating from the reactants in reactions 2 and 3, respectively.

Experimentally, the ligand dissociation energies were determined from T-CID experiments.^{12,133-141} The extraction of ligand dissociation energies from these experiments requires elaborate post-processing. The post-processing of the data includes modeling of ion-molecule collision dynamics, approximating a density-of-state function, and a sophisticated fitting procedure.¹³³ While an uncertainty is attached to each of the experimental ligand dissociation

energies, this uncertainty only accounts for the uncertainty of one measured quantity and for variations between independent data sets. It does not account for other uncertainties introduced during data post-processing such as the application of a single "effective" vibrational frequency when modeling the density-of-states function.¹³³

We calculate ligand dissociation energies at zero Kelvin as the difference of the sums of electronic and zero-point vibrational energies (ZPE) for the lowest-energy conformer of the reactant and for the two fragments. DFT ZPEs are known to be a good approximation because they are governed by frequencies of stiff vibrations for which the harmonic approximation works best and because of a fortunate error compensation which makes unscaled BP86 harmonic frequencies calculated with a triple-zeta (or larger) basis set with polarization functions on all atoms in general similar to experimental fundamental frequencies.¹⁴²⁻¹⁴⁴ Accordingly, we found¹² that the ZPE correction for reaction 9 determined with different density functionals scatters by 1.5 kJ mol⁻¹. Therefore, for a direct comparison of calculated and experimental dissociation energies, we subtract from the experimental data the ZPE difference calculated with BP86/def2-QZVPP from Ref. 12 (see Table 6 in the Supporting Information of that reference). Besides the approximation introduced by the electronic structure method itself and the harmonic ZPE contribution, an important approximation is introduced by relying on a specific molecular structure. In this work, each compound (reactants and fragments) is only represented by one conformer. This approximation is justified if the dissociation energy is considered at zero Kelvin, as is the case here, and each structure actually corresponds to the lowest-energy conformer. For several of the large structures (in particular, for reactions 2 and 3), conformational searches were carried out in Ref. 12 to identify the lowest-energy conformers.

4 Results and Discussion

4.1 Assessment of Multi-Configurational Character

Different proposals exist to define a diagnostic of the multi-configurational character of a molecule. Recently, we presented the $Z_{s(1)}$ diagnostic¹¹⁹ as a measure that is obtained from a multi-configurational wave function. It is calculated from the single-orbital entropies in a partially converged, but qualitatively correct, and therefore inexpensive DMRG wave function. In Ref. 119, we established guidelines regarding the applicability of single-reference methods based on the $Z_{s(1)}$ value. In general, single-reference meth-

Table 1: Multi-configurational $Z_{s(1)}$ diagnostic and single-configurational D_1 diagnostic from Ref. 29 for all molecules involved in reactions in the WCCR10 set. The reactants and products (charged and neutral fragments, respectively) are displayed in Figure 1.

Reaction	$Z_{s(1)}$		Reactant	D_1 (from Ref. 29)	
	Reactant	Products		Charged Fragment	Neutral Fragment
1	0.15	0.15	0.028	0.028	0.017
2	0.09	0.07	0.028	0.029	0.028
3	0.09	0.10	0.028	0.029	0.028
4	0.22	0.37	0.044	0.032	0.021
5	0.12	0.04	0.023	0.022	0.027
6	0.17	0.12	0.030	0.030	0.041
7	0.12	0.15	0.031	0.037	0.041
8	0.14	0.14	0.031	0.037	0.041
9	0.23	0.12 ^a	0.034	0.027	0.035
10	0.14	0.15	0.028	0.029	0.030

^a This diagnostic was evaluated with the final active space employed in the multi-configurational calculation (see also the Supporting Information).

ods will be appropriate when $Z_{s(1)} < 0.10$ and multi-reference methods will be required when $Z_{s(1)} > 0.20$. Single-reference methods such as CC with sufficiently high excitation degree may accurately describe cases which fall in the intermediate regime, $0.10 < Z_{s(1)} < 0.20$.

A popular measure that is, however, based on a single-reference wave function to be evaluated even for a potential multi-configurational case, is the D_1 diagnostic.¹⁴⁵ It is calculated from the matrix norm of the single-excitation amplitude vector of a CC wave function with single and double excitations. Janssen *et al.* suggested that $D_1 < 0.02$ indicates single-configurational character and $D_1 > 0.05$ indicates multi-configurational character.¹⁴⁵ In the intermediate regime, $0.02 < D_1 < 0.05$, caution is advised.¹⁴⁵ We present results for the $Z_{s(1)}$ diagnostic and for the D_1 diagnostic (obtained from CCSD amplitudes by Werner and collaborators²⁹) in Table 1.

The D_1 diagnostic indicates that all molecules involved in reactions in the WCCR10 set fall in the intermediate regime where we may assume that CCSD(T) calculations will yield reliable results ($0.022 < D_1 < 0.044$, see Table 1). The $Z_{s(1)}$ diagnostic also indicates that the majority of the molecules (fourteen out of twenty species) fall into an intermediate regime ($0.10 < Z_{s(1)} < 0.20$, see Table 1). Three species (reactants of reactions 2 and

3, and products of reaction 2) exhibit a $Z_{s(1)}$ value which is slightly lower than the threshold value of $Z_{s(1)} = 0.10$, and hence, these species can be classified as clear single-configurational cases. Consequently, multi-reference calculations are generally not required to obtain accurate electronic energy differences for eight out of the ten reactions in the WCCR10 set. The reactants of reactions 4 and 9, and the products of reaction 4 are species which exhibit nonnegligible static electron correlation according to the $Z_{s(1)}$ diagnostic ($0.22 < Z_{s(1)} < 0.37$). Hence, reactions 4 and 9 will be interesting targets for multi-reference perturbation theories.

4.2 Ab Initio Dissociation Energies

Figure 2 shows the WCCR10 ligand dissociation energies calculated with multi-reference perturbation theories: CASPT2, DMRG-SC-NEVPT2, and DMRG-PC-NEVPT2 (for numerical data see Table 3 in the Supporting Information).

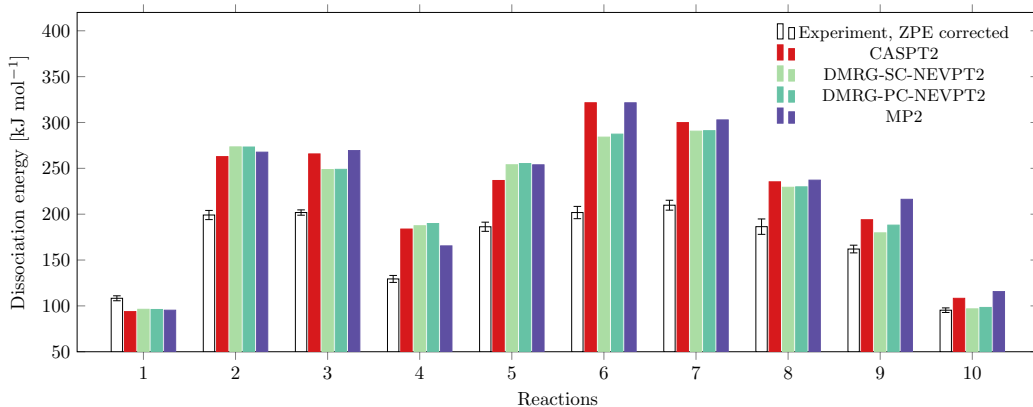


Figure 2: Comparison of ZPE-back corrected experimental and calculated ligand dissociation energies in kJ mol^{-1} . The ligand dissociation energies were calculated with multi-configurational perturbation theories (CASPT2, DMRG-SC-, and DMRG-PC-NEVPT2) and single-configurational Møller-Plesset perturbation theory (MP2). All results were obtained with an ANO-RCC basis set.

Given the low amount of static electron correlation for most species in the WCCR10 set, it is particularly interesting to compare multi-reference perturbation theory with the single-reference methods, in particular with MP2/ANO-RCC. For molecules with a low multi-configurational character, we expect the multi-reference perturbation theories to yield results close to

MP2/ANO-RCC, while a larger deviation is expected for molecules with increased static correlation. In agreement with this expectation, we observe the largest deviations between the CASPT2, DMRG-SC-NEVPT2, and DMRG-PC-NEVPT2 and the MP2/ANO-RCC results for reactions 4 and 9 which are the two reactions for which $Z_{s(1)} > 0.20$. The CASPT2, DMRG-SC-NEVPT2, and DMRG-PC-NEVPT2 results deviate from the MP2/ANO-RCC result by 18.4, 22.0, and 24.4 kJ mol⁻¹, respectively, for reaction 4 and by 22.2, 36.5, and 28.1 kJ mol⁻¹ for reaction 9. For the other reactions, for which $Z_{s(1)} < 0.20$, the deviations between the results obtained CASPT2, DMRG-SC-NEVPT2, and DMRG-PC-NEVPT2 and the MP2/ANO-RCC ligand dissociation energies are on average 4.9, 13.1, and 12.3 kJ mol⁻¹, respectively. The larger deviation of DMRG-SC-NEVPT2 and DMRG-PC-NEVPT2 results from the MP2/ANO-RCC data compared to CASPT2 is due to the Dyll Hamiltonian chosen as the zeroth-order Hamiltonian in NEVPT2. This Hamiltonian includes two-electron interactions in the active space. Therefore, it is capable of recovering more correlation energy already at zeroth order. The application of an IPEA shift of 0.25 a.u. for CASPT2 calculations leads, on average, to an increase of the ligand dissociation energies by about 4.5 kJ mol⁻¹ (see Table 3 in the Supporting Information).

Table 2: ZPE-back corrected experimental ligand dissociation energies and DLPNO-CCSD(T) ligand dissociation energies in kJ mol⁻¹. All DLPNO-CCSD(T) calculations were extrapolated to the complete basis set limit from single-point energies obtained with a cc-pVTZ(-PP) and a cc-pVQZ(-PP) basis set, the single-point calculations were carried out for BP86/def2-QZVPP and BP86-D3(0)/def2-QZVPP optimized structures.

Rct.	Experiment	Reference	DLPNO-CCSD(T)/ CBS//BP86/ def2-QZVPP	DLPNO-CCSD(T)/ CBS//BP86-D3(0)/ def2-QZVPP
1	108.3 ± 2.7	134	105.6	107.1
2	199.1 ± 5.0	135	238.2	265.1
3	201.8 ± 2.9	135	237.7	263.6
4	129.4 ± 3.8	12, 136	207.0	220.5
5	186.3 ± 5.0	12, 137	183.7	188.6
6	201.8 ± 6.7	138, 139	278.4	281.9
7	209.8 ± 5.4	138, 139	244.5	250.0
8	186.4 ± 8.4	138, 139	205.9	209.7
9	162.0 ± 4.2	140	151.0	152.2
10	95.3 ± 2.5	141	98.5	99.5

Table 2 additionally presents WCCR10 ligand dissociation energies obtained with DLPNO-CCSD(T) and the experimental results. On average, the DLPNO-CCSD(T)//BP86 results differ by 30.3 kJ mol⁻¹ from the experimental data and individual deviations may be as large as 77.6 kJ mol⁻¹ (reaction 4). The optimization of the WCCR10 structures with several density functionals without any dispersion correction resulted in nearly identical structures.¹² We, therefore, do not expect large effects on CC energies for those structures. We, however, found sizable differences between structures optimized with ordinary density functionals and structures optimized with dispersion-corrected density functionals.¹² Hence, we additionally evaluated DLPNO-CCSD(T) ligand dissociation energies for BP86-D3(0) optimized structures (see last column in Table 2). The disagreement with the experimental data increased compared to DLPNO-CCSD(T)//BP86: the mean absolute deviation of DLPNO-CCSD(T)//BP86-D3(0) complexation energies with respect to the experimental data is 38.0 kJ mol⁻¹ and the largest absolute deviation is 91.1 kJ mol⁻¹ (reaction 4). For all reactions, the DLPNO-CCSD(T)//BP86-D3(0) ligand dissociation energies are larger than the DLPNO-CCSD(T)//BP86 results. We observe the largest difference between the DLPNO-CCSD(T)//BP86-D3(0) and DLPNO-CCSD(T)//BP86 ligand dissociation energies for reactions 2, 3, and 4 (26.9, 25.9, and 13.5 kJ mol⁻¹, respectively). We should emphasize that one would expect that dispersion-corrected molecular structures should match well with those present in the gas phase of the mass spectrometer in which the experimental results were obtained.^{146,147}

In summary, the ligand dissociation energies calculated with DLPNO-CCSD(T) agree well with the experimental data for reaction 1, 5, and 10, while they are at least 19.4 kJ mol⁻¹ larger than the experimental ones for reactions 2, 3, 6, 7, and 8. Although reactions 1 and 10 feature small complexes and fragments, a comparison to reactions 6–8 shows that size cannot be considered a decisive cause for the good agreement. Our findings parallel those of Qu *et al.*¹⁷ and Pollice *et al.*¹⁸ who reported nonnegligible deviations of DLPNO-CCSD(T) ligand dissociation energies from results for different molecules.

We now turn our attention to the reaction with the largest $Z_{s(1)}$ measures, reactions 4 and 9. For reaction 9, the DLPNO-CCSD(T) ligand dissociation energy is by 11.0 kJ mol⁻¹ *smaller* than the measured energy. The CASPT2, DMRG-SC-NEVPT2, and DMRG-PC-NEVPT2 results are, by contrast, 32.0, 17.7, and 26.1 kJ mol⁻¹ *larger* than the experimental value, respectively. For reaction 4, we observe a very large difference of 77.6 kJ mol⁻¹ between the measured and the DLPNO-CCSD(T) energy. The CASPT2, DMRG-SC-NEVPT2, and DMRG-PC-NEVPT2 dissociation en-

ergies differ from the experimental data by 54.4, 58.0, and 60.4 kJ mol⁻¹, respectively. Unfortunately, reaction 4 is the reaction for which we were restricted to a valence double-zeta polarized basis set for non-metal atoms due to the large size of the reactant. From the comparison of MP2/ANO-RCC and MP2/CBS results, we can estimate the remaining basis set effect to be 40.9 kJ mol⁻¹ which is very large. We may conclude (although only cautiously for reaction 4) that for reactions 4 and 9, neither DLPNO-CCSD(T) nor the multi-reference perturbation theories yield satisfactory results. Reactions 9 and 4 might, hence, be valuable targets for multi-reference CC approaches at the basis-set limit.

4.3 Assessment of Density Functionals and Single-Reference Perturbation Theories

We now consider the accuracy of more approximate single-reference electronic structure models by comparing to the DLPNO-CCSD(T) ligand dissociation energies as a reference. All calculations were carried out for the BP86/def2-QZVPP optimized structures. Table 3 collects the mean absolute and largest absolute deviations (MAD and LAD, respectively) of ligand dissociation energies calculated with a selection of density functionals (PBE, BP86, BLYP, TPSS, M06-L, PBE0, B3LYP, TPSSh, and M06-2X) with and without D3 dispersion corrections, MP2, and SCS-MP2 with respect to the DLPNO-CCSD(T) results (see the Supporting Information for the numerical data).

Density functionals without dispersion correction. We first turn our attention to the results obtained with the PBE, BP86, BLYP, TPSS, PBE0, B3LYP, and TPSSh functionals. We observe the largest absolute deviation of the ligand dissociation energies calculated with any of these functionals to the DLPNO-CCSD(T) results for reaction 4. The ligand dissociation energy of reaction 4 is underestimated by 74.3 kJ mol⁻¹ (PBE0) to 146.4 kJ mol⁻¹ (BLYP, LADs in Table 3). In fact, the ligand dissociation energies for at least nine out of the ten reactions are smaller than the DLPNO-CCSD(T) results when they are calculated with one of these functionals, and overall, the obtained results deviate strongly from the DLPNO-CCSD(T) data (MAD > 29.7 kJ mol⁻¹, LAD > 74.3 kJ mol⁻¹). An unsatisfactory agreement of the ligand dissociation energies determined with non-dispersion-corrected density functionals with DLPNO-CCSD(T) energies is, however, expected due to the lack of attractive dispersion interactions in the (undissociated) complexes.

The Minnesota functionals M06-L and M06-2X describe dispersion inter-

Table 3: Mean absolute deviations (MAD) and largest absolute deviations (LAD) of ligand dissociation energies calculated with various approximate electronic structure models with respect to DLPNO-CCSD(T) data in kJ mol^{-1} . We indicate in parenthesis for which reaction the LAD was found. All DFT calculations were carried out with a def2-QZVPP basis set. We extrapolated cc-pVTZ(-PP) and cc-pVQZ(-PP) MP2 and SCS-MP2 results to the complete basis set limit.

Method	MAD	LAD	
PBE	32.5	96.3	(Rct. 4)
BP86	41.2	113.2	(Rct. 4)
BLYP	56.1	146.4	(Rct. 4)
TPSS	34.4	97.3	(Rct. 4)
M06-L	13.2	28.6	(Rct. 6)
PBE0	29.7	74.3	(Rct. 4)
B3LYP	47.0	112.2	(Rct. 4)
TPSSh	32.1	80.7	(Rct. 4)
M06-2X	21.4	41.3	(Rct. 6)
PBE-D3(BJ)	10.2	23.6	(Rct. 7)
BP86-D3(BJ)	17.3	31.5	(Rct. 5)
BLYP-D3(BJ)	9.2	17.5	(Rct. 6)
TPSS-D3(BJ)	10.6	25.0	(Rct. 7)
M06-L-D3(0)	7.7	25.4	(Rct. 6)
PBE0-D3(BJ)	4.3	9.1	(Rct. 9)
B3LYP-D3(BJ)	8.2	15.8	(Rct. 3)
TPSSh-D3(BJ)	10.8	21.1	(Rct. 5)
M06-2X-D3(0)	16.3	38.3	(Rct. 6)
SCS-MP2/CBS	16.8	29.7	(Rct. 4)
MP2/CBS	29.3	66.2	(Rct. 9)

actions to some degree by parametrization of a flexible functional form.⁹⁸ Accordingly, the deviation of the ligand dissociation energy for reaction 4 from the DLPNO-CCSD(T) result only amounts to 26.1 kJ mol^{-1} for M06-L and to 18.1 kJ mol^{-1} for M06-2X (compared to at least 74.3 kJ mol^{-1} for one of the other functionals). For the complete WCCR10 set, the meta-GGA functional M06-L exhibits the highest accuracy amongst all density functionals without dispersion corrections with an MAD of 13.2 kJ mol^{-1} , while M06-2X achieves an MAD of 21.4 kJ mol^{-1} . M06-L and M06-2X, however, still lead to too small ligand dissociation energies for nine out of the ten reactions in comparison to DLPNO-CCSD(T) (with the exceptions of reac-

tion 7 (M06-L) and reaction 1 (M06-2X)). M06 functionals do not reproduce the proper scaling of dispersive interactions with the sixth inverse power of the distance,¹⁰⁶ and hence, still underestimate the dispersion interactions for most reactions.

Møller-Plesset perturbation theories. In general, ordinary MP2/CBS does not perform significantly better than most density functionals for the WCCR10 set (MAD = 29.3 kJ mol⁻¹, LAD = 66.2 kJ mol⁻¹). In fact, MP2/CBS overestimates the ligand dissociation energies for all reactions but reaction 1 which is underestimated by 15.4 kJ mol⁻¹. For reactions 2–10, the MP2/CBS ligand dissociation energies are on average 30.8 kJ mol⁻¹ larger than the DLPNO-CCSD(T) results. SCS-MP2⁸³ corrects partially for shortcomings of MP2 by scaling the same-spin and opposite-spin components in MP2 differently. For the complete WCCR10 set, SCS-MP2/CBS achieves an MAD of 16.8 kJ mol⁻¹ and an LAD of 29.7 kJ mol⁻¹. Hence, the overall reliability of SCS-MP2/CBS is worse than what we found for the M06-L functional, but is still on par with several dispersion-corrected density functionals.

Dispersion-corrected density functionals. The application of dispersion corrections in DFT has become a *de facto* standard and we investigate several dispersion corrections in more detail. A popular way to account for dispersion interactions in DFT calculations is the application of semiclassical D3 dispersion corrections.⁸¹ The inclusion of D3 corrections leads to an increase of the predicted ligand dissociation energies in comparison to the ones calculated without D3 corrections for all reactions in the WCCR10 set and for all functionals. The resulting B3LYP-D3(BJ) ligand dissociation energies agree better with the DLPNO-CCSD(T) energies than the B3LYP ones for every single reaction. For the PBE0, BLYP, PBE, BP86, TPSS, and TPSSh functionals, the agreement is improved for at least seven out of the ten reactions when invoking D3 corrections. These improvements may be enormous in some cases, e.g., the deviation from the DLPNO-CCSD(T) result for reaction 4 decreases between 59.7 kJ mol⁻¹ (TPSSh vs. TPSSh-D3(BJ)) and 145.9 kJ mol⁻¹ (BLYP vs. BLYP-D3(BJ)) when including D3 corrections compared to the one for the uncorrected functionals. For M06-L and M06-2X, we also observe a decrease of the deviations for at least nine out of the ten reactions when including D3 corrections. Note, however, how the M06 series of functionals show similar MAD with and without the D3 dispersion correction owing to the fact that the uncorrected functionals already include dispersive interactions to some degree through their parametrization. For the

complete WCCR10 set, the best agreement with the DLPNO-CCSD(T) data was found for PBE0-D3(BJ) (MAD = 4.3 kJ mol⁻¹, LAD = 9.1 kJ mol⁻¹). Two other dispersion-corrected functionals (BLYP-D3(BJ), B3LYP-D3(BJ)) yield MAD’s below 10 kJ mol⁻¹ and LAD’s below 20 kJ mol⁻¹. In general, the mean and largest absolute deviations of the results obtained with dispersion-corrected density functionals are smaller than the ones obtained for their non-dispersion-corrected counterparts for all functionals considered and do not exceed 17.3 kJ mol⁻¹ and 38.3 kJ mol⁻¹, respectively (MAD of BP86-D3(BJ) and LAD of M06-2X-D3(0), see also Table 3).

The D3 corrections incorporate fit parameters which introduce a prediction uncertainty.¹⁴⁸ We estimate the uncertainties of the B3LYP-D3(BJ) dispersion energies with the BOOTD3 program.¹⁴⁸ As reported in Ref. 148, the uncertainty of (absolute) dispersion energies grows with molecular size. Not surprisingly, we observe the largest uncertainty of an absolute dispersion energy for the largest molecule in the WCCR10 set, namely for the reactant of reaction 4 with an absolute B3LYP-D3(BJ) dispersion energy of -1260.4 kJ mol⁻¹ with a standard deviation of 49.6 kJ mol⁻¹ (see Table 18 in the Supporting Information). The uncertainty of the dispersion contributions to the B3LYP-D3(BJ) reaction energies is, however, much smaller, i.e., less than 2.7 kJ mol⁻¹ for eight out of the ten reactions. Larger uncertainties we found for reactions 4 and 5 (4.5 and 6.6 kJ mol⁻¹, respectively).

Furthermore, the D3 dispersion corrections only depend on atom positions, but not on the electron density (or even the charge) of the molecule (see, e.g., Ref. 149). Transition-metal complexes can, however, show a variety of low-lying electronic states for similar molecular structures (e.g., in case of different spin states). We therefore also investigated other types of dispersion corrections for the B3LYP functional: XDM, NL, and SCNL (see Figure 3).

The results obtained with B3LYP-SCNL and B3LYP-NL differ at most by 1.7 kJ mol⁻¹ (reaction 4) for the reactions in the WCCR10 set. Apparently, the electron density is not affected severely by the inclusion of nonlocal dispersion corrections of this type. Figure 3 illustrates that the inclusion of any type of dispersion correction to the B3LYP ligand dissociation energies leads to an improved agreement with the DLPNO-CCSD(T) results for every single reaction. Nevertheless, we still encounter sizeable deviations. The deviations of B3LYP-D3(BJ) ligand dissociation energies from DLPNO-CCSD(T) energies exceed 11.6 kJ mol⁻¹ for reactions 2, 3, 4, and 6. Similarly large errors are encountered for reactions 2 and 3 when the ligand dissociation energies are calculated with B3LYP-SCNL (14.9 and 18.1 kJ mol⁻¹, respectively). The B3LYP-XDM ligand dissociation energies tend to be too small so that the ligand dissociation energies for reactions 6 and 10 are un-

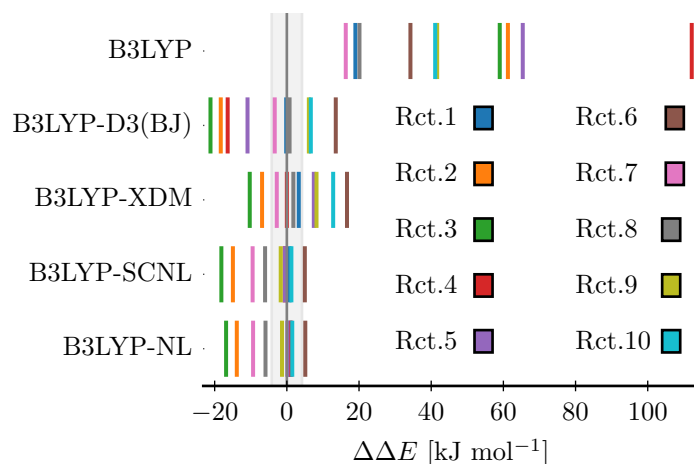


Figure 3: Deviation of electronic ligand dissociation energies ΔE in kJ mol^{-1} calculated with (dispersion corrected) B3LYP from DLPNO-CCSD(T) values. All (dispersion-corrected) B3LYP energies were calculated with a def2-QZVPP basis set for BP86/def2-QZVPP optimized structures. The gray region indicates the region where chemical accuracy is achieved, i.e., where deviations from the DLPNO-CCSD(T) data are smaller than 4.2 kJ mol^{-1} .

derestimated by 16.7 and 12.8 kJ mol^{-1} , respectively. Overall, the MADs of B3LYP-D3(BJ), B3LYP-NL, B3LYP-SCNL, and B3LYP-XDM results with respect to the DLPNO-CCSD(T) ligand dissociation energies are between 5.6 kJ mol^{-1} (B3LYP-NL) and 8.2 kJ mol^{-1} (B3LYP-D3(BJ)) compared to an MAD of 47.0 kJ mol^{-1} for the dispersion-uncorrected B3LYP results.

5 Possible Origins of Discrepancies between Calculated and Experimental Ligand Dissociation Energies

At present, it is difficult to shed more light on the source of discrepancies between theory and experiment as neither is without limitations. However, in view of the different quantum chemical approaches considered in this paper, we may draw some conclusions after having put together more pieces of the puzzle.

First of all, we emphasize that the two other approaches (XDM and NL) to incorporate dispersion corrections into dispersion-free density functionals yield similar results compared to the semiclassical dispersion corrections by

Grimme and to CC calculations which was also noted for other transition-metal complexes.¹⁵⁰

The correlation energy in CC calculations is known to converge only slowly with the basis-set size which can introduce sizable errors. Ma *et al.*²⁹ obtained PNO-LCCSD-F12b/VTZ-F12 ligand dissociation energies for the WCCR10 set which are well converged with respect to the basis-set size; the deviation of PNO-LCCSD-F12b/VTZ-F12 from PNO-LCCSD-F12b/VDZ-F12 results does not exceed 2.9 kJ mol⁻¹. Our DLPNO-CCSD results deviate on average by 4.8 kJ mol⁻¹ (at most by 8.2 kJ mol⁻¹ for reaction 2, Table 5 in the Supporting Information) from the PNO-LCCSD-F12b/VTZ-F12 results which indicates that the former are converged reasonably well with respect to the basis-set size. A larger basis set would, however, be desirable especially for reactions 2, 3, and 4.

The comparison with PNO-LCCSD(T)-F12b/VTZ-F12 data⁸² highlights an issue associated with DLPNO-CCSD(T) calculations. While our DLPNO-CCSD(T) data deviate by less than 1.6 kJ mol⁻¹ from PNO-LCCSD(T)-F12b energies for six out of the ten reactions, larger deviations of up to 18.0 kJ mol⁻¹ were found for reaction 7. We can attribute these differences to the applied PNO thresholds; the deviations for reactions 1, 7, and 9 decrease from 5.9, 18.0, and 5.0 kJ mol⁻¹ to 1.8, 10.9, and 0.1 kJ mol⁻¹, respectively, when TIGHTPNO settings are applied in the DLPNO-CCSD(T) calculations (see Table 7 in the Supporting Information). Evidently, even tighter PNO thresholds would be desirable for reaction 7. The quadruple-zeta basis set and TIGHTPNO settings are already very costly in terms of computing time. This highlights the benefits of explicitly correlated methods which converge faster with respect to the basis-set size. We emphasize that the deviations to the experimental data also persist when comparing against PNO-LCCSD(T)-F12b results⁸² and that both methods, DLPNO-CCSD(T) and PNO-LCCSD(T)-F12, were found to generate much smaller deviations in other reference data sets.^{19,20,26-29,94}

Apart from intrinsic limitations of electronic structure methods, we must keep in mind that the molecular structure model is a possible cause for the origin of discrepancies between theory and experiment. Different neutral dissociation products are, e.g., possible for reactions 6–8 (e.g., 1,1-dimethyldiazene (as assumed in this study), *cis*-1,2-dimethyldiazene, *trans*-1,2-dimethyldiazene, or formaldehyde methylhydrazone) that convert into each other through unimolecular re-arrangements of methyl groups.^{138,139} It cannot (and does not need to) be determined by mass spectrometry which of these products is formed. A choice for one structures is, however, required to carry out electronic structure calculations. The most likely dissociation product for reactions 6–8 was identified in DFT calculations^{138,139} which may

present issues according to our work in Ref. 12 and Section 4.3. Additionally, the consideration of structures which do not correspond to the lowest-energy conformers may be a source of error. Although, for the structures reported in Ref. 12 conformational sampling was considered to a certain degree (see the Supporting Information of that paper), further investigations might be appropriate.

Furthermore, modeling assumptions exist in the post-processing protocol of the experimental data. Several factors in this post-processing protocol were discussed^{133, 135, 136, 138, 139, 141} which possibly affect the experimentally determined ligand dissociation energies for the reactions in the WCCR10 set as we shall review in the following.

The experimental ligand dissociation energies vary slightly with the number of assumed internal rotors (input parameter).¹³³ Although this protocol was only verified for ions with up to fifty atoms,¹³³ it is better fulfilled, the larger the dissociating molecules become. This is due to the fact that the ratio of the moments of inertia between reactant and dissociation products and consequently the rigid-rotor partition functions tends to one for large reactants. For reaction 4, the largest and smallest ligand dissociation energies determined with different numbers of internal rotors vary¹³⁶ by 10 kJ mol⁻¹ which is much smaller than the deviation of 77.6 kJ mol⁻¹ between the experimental and the DLPNO-CCSD(T) data.

The post-processing strategy necessitates a choice between a "tight" and a "loose" transition-state model.¹³³ A tight transition-state model is assumed to represent reactions well in which an intramolecular rearrangement is rate limiting, whereas a loose transition-state model is appropriate when a dissociation process determines the rate. The overall dissociation reaction may, however, involve multiple steps and it is not *a priori* clear whether the rate-limiting step is the ligand dissociation reaction itself or, e.g., an intramolecular rearrangement preceding ligand dissociation. Hence, prior knowledge is required to choose either the loose or the tight transition-state model.¹⁴¹ Generally, the experimental ligand dissociation energy turns out to be larger when assuming a loose transition state than when assuming a tight one. For all reactions in the WCCR10 set, the loose transition-state model was chosen during the post processing yielding a maximum value for the dissociation energy. Therefore, the large observed deviations between experimental and CC data cannot be explained by the choice of transition-state model because the CC results are even larger than the experimental energies for the reactions for which we observe large discrepancies (reactions 2, 3, 6, 7, and 8). Hence, the differences between measured and calculated energies would become even larger when the tight transition-state model would be selected in the post-processing step.

In addition, further sources of uncertainties in the post-processing protocol may exist. For instance, the reactant is thermalized at 343 K¹³³ which is going to result in the formation of a conformational equilibrium. This implies that the reactant may collide with the collision gas in various conformations and the reported ligand dissociation energies represent some sort of average over the accessible conformations (even if fast energy redistribution and relaxation may populate only few lowest-energy conformers).

To address the reliability of the post-processing protocol for large complexes, Pollice *et al.*¹⁸ devised an example which is largely independent of the assumptions in this protocol. These authors synthesized a proton-bound dimer which can undergo two alternative dissociation reactions (hydrogen bond cleavage or O-NO bond cleavage) upon collision (see Figure 4). Only the products which result from a hydrogen bond cleavage reaction were observed in the mass spectrometer. The DLPNO-CCSD(T) bond dissociation energy for the hydrogen bond cleavage was, however, found to be larger than the one for the O-NO bond cleavage from which they concluded that the wrong product is predicted.¹⁸ This experimental finding puts an unexpectedly large deviation of at least 21 kJ mol⁻¹ on the calculated DLPNO-CCSD(T) dissociation energies. However, we should also note that the theoretical prediction of a major product requires the determination of free energy differences at the respective temperature which has recently been emphasized by Carpenter and co-workers.¹⁵¹ Carpenter *et al.* studied the dissociation of a para-nitrobenzylpyridinium cation in T-CID experiments.¹⁵¹ The bond dissociation energy associated with the reaction yielding the major product was larger than the one associated with the reaction yielding the minor product. Carpenter *et al.* rationalized why the major product was observed by including the entropies associated with the dissociation processes in their analysis.¹⁵¹

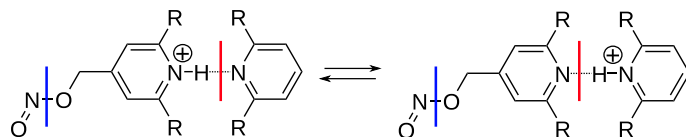


Figure 4: Lewis structures of a proton-bound dimer (R denotes 3,5-di-*tert*-butyl-phenyl substituents) which can undergo either homolytic O-NO bond cleavage (blue line) or hydrogen-bond cleavage (red line).

Furthermore, the comparison of the theoretical dissociation pathways with the experimental result assumes full statistical intramolecular vibrational energy redistribution (IVR). This assumption is fulfilled only if the dissociation occurs on a slower timescale than IVR. If the dissociation competes

with IVR, a ligand with a larger collision cross-section is more likely to dissociate. Dissociation reactions do not compete with IVR in general, but cases in which a competition occurs have been reported for small molecules^{152, 153} and medium-sized non-covalently bound ions.¹⁵⁴ For the example in Figure 4, the collision cross-section of the pyridine monomer dissociating as a result of the hydrogen bond cleavage might be much larger than that of NO, and hence, hydrogen bond cleavage could be preferred. However, the experimental set-up in Refs. 152 and 153 promotes fast reactions and non-ergodic behavior, which is not necessarily the case for the comparatively long-lived collision complexes produced in T-CID experiments.

To conclude, although we have carefully re-examined possible sources of uncertainty in the electronic structure models (see also the Supporting Information) and in experiment, none of the usual suspects appear to be accountable for the large deviation of high-level CC data from the experimental energies.

6 Conclusions

We revisited the WCCR10 set of ten ligand dissociation energies to provide results from correlated single- and multi-reference wave function methods and to further investigate the role of dispersion interactions.

We first assessed the multi-configurational character of all molecules in the WCCR10 set with our multi-reference $Z_{s(1)}$ diagnostic which is based on a qualitatively correct multi-configurational wave function. Two reactions (reactions 4 and 9) turned out to involve molecules which exhibit nonnegligible static electron correlation. Our results showed that these two reactions were even challenging for multi-reference perturbation theories and satisfactory agreement with the experimental data was not achieved for either reaction. These two reactions therefore represent interesting targets for other multi-reference methods such as multi-reference coupled-cluster approaches at the basis-set limit.

After ascertaining that single-reference approaches are adequate for eight out of the ten reactions in the WCCR10 set, we carried out DLPNO-CCSD(T) calculations. We were able to achieve a reasonable agreement with the experimental data for three reactions (reactions 1, 5, and 10). For the other five reactions (reactions 2, 3, 6, 7, and 8), which involve single-configurational complexes and fragments according to the $Z_s(1)$ diagnostic, we observed deviations between 19.4 and 76.6 kJ mol⁻¹ from the experimental energies. We ensured that our coupled-cluster results were essentially converged with respect to the basis-set size by comparison of our DLPNO-CC data to ex-

plicitly correlated CC results from Refs. 29, 82. The comparison of our DLPNO-CCSD(T) data with explicitly correlated CCSD(T) data from Ref. 82 showed that the application of tight PNO thresholds might be required for accurate results in some cases (reaction 7). We also addressed the structural uncertainty by comparing results obtained for BP86 and BP86-D3(0) structures. Contrary to ones’ expectation, the deviation of the DLPNO-CCSD(T) results from the experimental data increased even further when BP86-D3(0) instead of BP86 structures were chosen. Neither the basis-set size nor the threshold criteria nor the structural uncertainties appear to be able to account for the very large discrepancies between coupled-cluster and experimental data. While we discussed several possible causes for the observed deviations, it is currently not possible to pinpoint the cause because there is simply not enough data available to detect trends. Hence, it is indispensable to consider more experimental gas-phase data on binding energies of medium-sized to large molecules in order to finally track down the sources of these nagging discrepancies.

For the single-configurational molecules, we compared the results of density-functional calculations and single-reference perturbation theories with DLPNO-CCSD(T) data. We generally cannot recommend the application of single-reference perturbation theories in this context because the overall reliability of MP2 and SCS-MP2 (MAD of 29.3 kJ mol⁻¹ and 16.8 kJ mol⁻¹, respectively) was worse than what we found for several (dispersion-corrected) density functionals. Multi-reference perturbation theories, when applied for single-configurational species, yielded results close to single-reference perturbation theories, and hence, do also not achieve a good agreement with the DLPNO-CCSD(T) data. We found that M06-L results exhibited the lowest mean absolute deviation (13.2 kJ mol⁻¹) out of the results obtained with nine pure density functionals (PBE, BP86, BLYP, TPSS, M06-L, PBE0, B3LYP, TPSSh, M06-2X). This may be rationalized by the fact that the Minnesota functionals describe dispersion interactions to some degree through their parametrization in contrast to the other functionals (PBE, BP86, BLYP, TPSS, PBE0, B3LYP, TPSSh).

Naturally, an adequate description of dispersion interactions is crucial to yield accurate *gas-phase* ligand dissociation energies for large transition metal complexes. The agreement with the DLPNO-CCSD(T) results improved significantly for every density functional when semiclassical D3 dispersion corrections were considered. We found that the D3 corrections for the B3LYP functional agreed well with other density-dependent dispersion corrections (B3LYP-NL, B3LYP-SCNL, B3LYP-XDM) which may be taken as further evidence that they are reliable. We explicitly assessed the uncertainty of the B3LYP-D3(BJ) relative dispersion energies with BOOTD3¹⁴⁸ which is only

2.0 kJ mol⁻¹ on average and which does not exceed 6.6 kJ mol⁻¹ for the WCCR10 set.

For the whole WCCR10 set, DLPNO-CCSD(T) and all D3-dispersion-corrected density functionals yielded similar results. The results obtained with PBE0-D3(BJ) agreed very well with the DLPNO-CCSD(T) data. The PBE0-D3(BJ) results deviated at most by 9.1 kJ mol⁻¹ and on average by 4.3 kJ mol⁻¹ from the DLPNO-CCSD(T) energies. A system-focused density-functional parametrization in combination with rigorous error estimation^{155,156} could reduce these already small errors further when highly accurate results are required as, for instance, for the elucidation of reaction kinetics.¹⁵⁷

Acknowledgements

This work was supported by the Schweizerischer Nationalfonds (Project No. 200020_169120). L.F. acknowledges the Austrian Science Fund FWF for a Schrödinger fellowship (Project No. J 3935). We are grateful to Prof. Peter Chen for helpful discussions.

Supporting Information

Details on parameter-dependence studies, orbital entanglement diagrams, the active space selection for multi-configurational calculations, as well as total electronic energies and DFT and MP2 ligand dissociation energies can be found in the Supporting Information. This information is available free of charge via the Internet at <http://pubs.acs.org/>.

References

- [1] Determan, J. J.; Poole, K.; Scalmani, G.; Frisch, M. J.; Janesko, B. G.; Wilson, A. K. Comparative Study of Nonhybrid Density Functional Approximations for the Prediction of 3d Transition Metal Thermochemistry, *J. Chem. Theory Comput.* **2017**, *13*, 4907–4913.
- [2] Aebersold, L. E.; Yuwono, S. H.; Schoendorff, G.; Wilson, A. K. Efficacy of Density Functionals and Relativistic Effective Core Potentials for Lanthanide-Containing Species: The Ln54 Molecule Set, *J. Chem. Theory Comput.* **2017**, *13*, 2831–2839.

- [3] Ashley, D. C.; Jakubikova, E. Ironing out the photochemical and spin-crossover behavior of Fe(II) coordination compounds with computational chemistry, *Coord. Chem. Rev.* **2017**, *337*, 97–111.
- [4] Gani, T. Z. H.; Kulik, H. J. Unifying Exchange Sensitivity in Transition-Metal Spin-State Ordering and Catalysis through Bond Valence Matrices, *J. Chem. Theory Comput.* **2017**, *13*, 5443–5457.
- [5] Grimmel, S.; Schoendorff, G.; Wilson, A. K. Gauging the Performance of Density Functionals for Lanthanide-Containing Molecules, *J. Chem. Theory Comput.* **2016**, *12*, 1259–1266.
- [6] Swart, M.; Gruden, M. Spinning around in Transition-Metal Chemistry, *Acc. Chem. Res.* **2016**, *49*, 2690–2697.
- [7] Ioannidis, E. I.; Kulik, H. J. Towards quantifying the role of exact exchange in predictions of transition metal complex properties, *J. Chem. Phys.* **2015**, *143*, 034104.
- [8] Cramer, C. J.; Truhlar, D. G. Density Functional Theory for Transition Metals and Transition Metal Chemistry, *Phys. Chem. Chem. Phys.* **2009**, *11*, 10757–10816.
- [9] Tekarli, S. M.; Drummond, M. L.; Williams, T. G.; Cundari, T. R.; Wilson, A. K. Performance of Density Functional Theory for 3d Transition Metal-Containing Complexes: Utilization of the Correlation Consistent Basis Sets, *J. Phys. Chem. A* **2009**, *113*, 8607–8614.
- [10] Furche, F.; Perdew, J. P. The Performance of Semilocal and Hybrid Density Functionals in 3d Transition-Metal Chemistry, *J. Chem. Phys.* **2006**, *124*, 044103.
- [11] Salomon, O.; Reiher, M.; Hess, B. A. Assertion and validation of the performance of the B3LYP* functional for the first transition metal row and the G2 test set, *J. Chem. Phys.* **2002**, *117*, 4729–4737.
- [12] Weymuth, T.; Couzijn, E. P. A.; Chen, P.; Reiher, M. New Benchmark Set of Transition-Metal Coordination Reactions for the Assessment of Density Functionals, *J. Chem. Theory Comput.* **2014**, *10*, 3092–3103.
- [13] Weymuth, T.; Reiher, M. Systematic Dependence of Transition-Metal Coordination Energies on Density-Functional Parametrizations, *Int. J. Quantum Chem.* **2015**, *115*, 90–98.

- [14] Perdew, J. P. Density-Functional Approximation for the Correlation Energy of the Inhomogeneous Electron Gas, *Phys. Rev. B* **1986**, *33*, 8822–8824.
- [15] Yu, H. S.; He, X.; Truhlar, D. G. MN15-L: A New Local Exchange-Correlation Functional for Kohn–Sham Density Functional Theory with Broad Accuracy for Atoms, Molecules, and Solids, *J. Chem. Theory Comput.* **2016**, *12*, 1280–1293.
- [16] Kobylanskii, I. J.; Widner, F. J.; Kräutler, B.; Chen, P. Co–C Bond Energies in Adenosylcobinamide and Methylcobinamide in the Gas Phase and in Silico, *J. Am. Chem. Soc.* **2013**, *135*, 13648–13651.
- [17] Qu, Z.; Hansen, A.; Grimme, S. Co–C Bond Dissociation Energies in Cobalamin Derivatives and Dispersion Effects: Anomaly or Just Challenging?, *J. Chem. Theory Comput.* **2015**, *11*, 1037–1045.
- [18] Pollice, R.; Bot, M.; Kobylanskii, I. J.; Shenderovich, I.; Chen, P. Attenuation of London Dispersion in Dichloromethane Solutions, *J. Am. Chem. Soc.* **2017**, *139*, 13126–13140.
- [19] Minenkov, Y.; Chermak, E.; Cavallo, L. Accuracy of DLPNO–CCSD(T) Method for Noncovalent Bond Dissociation Enthalpies from Coinage Metal Cation Complexes, *J. Chem. Theory Comput.* **2015**, *11*, 4664–4676.
- [20] Sparta, M.; Neese, F. Chemical Applications Carried out by Local Pair Natural Orbital Based Coupled-Cluster Methods, *Chem. Soc. Rev.* **2014**, *43*, 5032–5041.
- [21] Tew, D. P.; Klopper, W.; Neiss, C.; Hättig, C. Quintuple- ζ quality coupled-cluster correlation energies with triple- ζ basis sets, *Phys. Chem. Chem. Phys.* **2007**, *9*, 1921–1930.
- [22] Bartlett, R. J. The coupled-cluster revolution, *Mol. Phys.* **2010**, *108*, 2905–2920.
- [23] Klopper, W.; Bachorz, R. A.; Hättig, C.; Tew, D. P. Accurate computational thermochemistry from explicitly correlated coupled-cluster theory, *Theor. Chem. Acc.* **2010**, *126*, 289–304.
- [24] Eriksen, J. J.; Matthews, D. A.; Jørgensen, P.; Gauss, J. Assessment of the accuracy of coupled cluster perturbation theory for open-shell systems. I. Triples expansions, *J. Chem. Phys.* **2016**, *144*, 194102.

- [25] Tajti, A.; Szalay, P. G.; Csaszar, A. G.; Kállay, M.; Gauss, J.; Valeev, E.; Flowers, B. A.; Vazquez, J.; Stanton, J. F. HEAT: High accuracy extrapolated ab initio thermochemistry, *J. Chem. Phys.* **2004**, *121*, 11599.
- [26] Riplinger, C.; Neese, F. An Efficient and near Linear Scaling Pair Natural Orbital Based Local Coupled Cluster Method, *J. Chem. Phys.* **2013**, *138*, 034106.
- [27] Riplinger, C.; Sandhoefer, B.; Hansen, A.; Neese, F. Natural Triple Excitations in Local Coupled Cluster Calculations with Pair Natural Orbitals, *J. Chem. Phys.* **2013**, *139*, 134101.
- [28] Schwilk, M.; Ma, Q.; Köppl, C.; Werner, H.-J. Scalable Electron Correlation Methods. 3. Efficient and Accurate Parallel Local Coupled Cluster with Pair Natural Orbitals (PNO-LCCSD), *J. Chem. Theory Comput.* **2017**, *12*, 3650–3675.
- [29] Ma, Q.; Schwilk, M.; Köppl, C.; Werner, H.-J. Scalable Electron Correlation Methods. 4. Parallel Explicitly Correlated Local Coupled Cluster with Pair Natural Orbitals (PNO-LCCSD-F12), *J. Chem. Theory Comput.* **2017**, *13*, 4871–4896.
- [30] Hanauer, M.; Köhn, A. Pilot applications of internally contracted multireference coupled cluster theory, and how to choose the cluster operator properly, *J. Chem. Phys.* **2011**, *134*, 204111.
- [31] Evangelista, F. A.; Gauss, J. An orbital-invariant internally contracted multireference coupled cluster approach, *J. Chem. Phys.* **2011**, *134*, 114102.
- [32] Köhn, A.; Hanauer, M.; Mück, L. A.; Jagau, T.-C.; Gauss, J. State-specific multireference coupled-cluster theory, *WIREs Comput. Mol. Sci.* **2013**, *3*, 176–1997.
- [33] Jeziorski, B.; Monkhorst, H. J. Coupled-cluster method for multide-terminantal reference states, *Phys. Rev. A* **1981**, *24*, 1668–1681.
- [34] Hanrath, M. An exponential multireference wave-function ansatz, *J. Chem. Phys.* **2005**, *123*, 084102.
- [35] Das, S.; Kállay, M.; Mukherjee, D. Superior performance of Mukherjee’s state-specific multi-reference coupled-cluster theory at the singles and doubles truncation scheme with localized active orbitals, *Chem. Phys.* **2012**, *392*, 83–89.

- [36] Roos, B. O.; Taylor, P. R.; Siegbahn, P. E. M. A complete active space SCF method (CASSCF) using a density matrix formulated super-CI approach, *Chem. Phys.* **1980**, *48*, 157–173.
- [37] Olsen, J. The CASSCF method: A perspective and commentary, *Int. J. Quantum Chem.* **2011**, *111*, 3267–3272.
- [38] Stein, C. J.; Reiher, M. Automated Selection of Active Orbital Spaces, *J. Chem. Theory Comput.* **2016**, *12*, 1760–1771.
- [39] Stein, C. J.; von Burg, V.; Reiher, M. The Delicate Balance of Static and Dynamic Electron Correlation, *J. Chem. Theory Comput.* **2016**, *12*, 3764–3773.
- [40] Stein, C. J.; Reiher, M. Automated Identification of Relevant Frontier Orbitals for Chemical Compounds and Processes, *CHIMIA* **2017**, *71*, 170–176.
- [41] White, S. R. Density Matrix Formulation for Quantum Renormalization Groups, *Phys. Rev. Lett.* **1992**, *69*, 2863–2866.
- [42] White, S. R. Density-matrix algorithms for quantum renormalization groups, *Phys. Rev. B* **1993**, *48*, 10345.
- [43] Marti, K. H.; Reiher, M. The Density Matrix Renormalization Group Algorithm in Quantum Chemistry, *Z. Phys. Chem.* **2010**, *224*, 583–599.
- [44] Chan, G. K.-L.; Sharma, S. The Density Matrix Renormalization Group in Quantum Chemistry, *Ann. Rev. Phys. Chem.* **2011**, *62*, 465–481.
- [45] Olivares-Amaya, R.; Hu, W.; Nakatani, N.; Sharma, S.; Yang, J.; Chan, G. K.-L. The ab-initio density matrix renormalization group in practice, *J. Chem. Phys.* **2015**, *142*, 034102.
- [46] Legeza, Ö.; Noack, R.; Sólyom, J.; Tincani, L. Applications of Quantum Information in the Density-Matrix Renormalization Group, *Lect. Notes Phys.* **2008**, *739*, 653–664.
- [47] Chan, G. K.-L.; Dorando, J. J.; Ghosh, D.; Hachmann, J.; Neuscamman, E.; Wang, H.; Yanai, T. An Introduction to the Density Matrix Renormalization Group Ansatz in Quantum Chemistry, *Prog. Theor. Chem. Phys.* **2008**, *18*, 49–65.

- [48] Chan, G. K.-L.; Zgid, D. The Density Matrix Renormalization Group in Quantum Chemistry, *Annu. Rep. Comput. Chem.* **2009**, *5*, 149–162.
- [49] Marti, K. H.; Reiher, M. New Electron Correlation Theories for Transition Metal Chemistry, *Phys. Chem. Chem. Phys.* **2011**, *13*, 6750–6759.
- [50] Schollwöck, U. The Density-Matrix Renormalization Group in the Age of Matrix Product States, *Annals of Physics* **2011**, *326*, 96–192.
- [51] Kurashige, Y. Multireference Electron Correlation Methods with Density Matrix Renormalisation Group Reference Functions, *Mol. Phys.* **2014**, *112*, 1485–1494.
- [52] Wouters, Sebastian,; Van Neck, Dimitri, The Density Matrix Renormalization Group for ab initio Quantum Chemistry, *Eur. Phys. J. D* **2014**, *68*, 272.
- [53] Yanai, T.; Kurashige, Y.; Mizukami, W.; Chalupský, J.; Lan, T. N.; Saitow, M. Density Matrix Renormalization Group for ab initio Calculations and Associated Dynamic Correlation Methods: A Review of Theory and Applications, *Int. J. Quantum Chem.* **2015**, *115*, 283–299.
- [54] Szalay, S.; Pfeiffer, M.; Murg, V.; Barcza, G.; Verstraete, F.; Schneider, R.; Legeza, Ö. Tensor Product Methods and Entanglement Optimization for ab initio Quantum Chemistry, *Int. J. Quantum Chem.* **2015**, *115*, 1342–1391.
- [55] Knecht, S.; Hedegård, E. D.; Keller, S.; Kovyrshin, A.; Ma, Y.; Muolo, A.; Stein, C. J.; Reiher, M. New Approaches for ab initio Calculations of Molecules with Strong Electron Correlation, *Chimia* **2016**, *70*, 244–251.
- [56] Chan, G. K.-L.; Keselman, A.; Nakatani, N.; Li, Z.; White, S. R. Matrix Product Operators, Matrix Product States, and ab initio Density Matrix Renormalization Group Algorithms, *J. Chem. Phys.* **2016**, *145*, 014102.
- [57] Andersson, K.; Malmqvist, P.-Å.; Roos, B. O.; Sadlej, A. J.; Wolinski, K. CASPT2: Second-Order Perturbation Theory with a CASSCF Reference Function, *J. Phys. Chem.* **1990**, *94*, 5483–5488.
- [58] Anderson, M. W.; Occelli, M. L.; Klinowski, J. Carbon-13 and proton magic-angle-spinning NMR studies of the conversion of methanol over offretite/erionite intergrowths, *J. Phys. Chem.* **1992**, *96*, 388–392.

- [59] Angeli, C.; Cimiraglia, R.; Evangelisti, S.; Leininger, T.; Malrieu, J.-P. Introduction of N-Electron Valence States for Multireference Perturbation Theory, *J. Chem. Phys.* **2001**, *114*, 10252.
- [60] Angeli, C.; Cimiraglia, R.; Malrieu, J.-P. N-Electron Valence State Perturbation Theory: A Spinless Formulation and an Efficient Implementation of the Strongly Contracted and of the Partially Contracted Variants, *J. Chem. Phys.* **2002**, *117*, 9138–9153.
- [61] Angeli, C.; Cimiraglia, R.; Malrieu, J.-P. N-electron valence state perturbation theory: a fast implementation of the strongly contracted variant, *Chem. Phys. Lett.* **2001**, *350*, 297–305.
- [62] Roca-Sanjuán, D.; Aquilante, F.; Lindh, R. Multiconfiguration second-order perturbation theory approach to strong electron correlation in chemistry and photochemistry, *WIREs Comput. Mol. Sci.* **2011**, *2*, 585–603.
- [63] Aquilante, F.; Malmqvist, P.-Å.; Pedersen, T. B.; Ghosh, A.; Roos, B. O. Cholesky Decomposition-Based Multiconfiguration Second-Order Perturbation Theory (CD-CASPT2): Application to the Spin-State Energetics of Co^{III}(Diiminato)(NPh), *J. Chem. Theory Comput.* **2008**, *4*, 694–702.
- [64] Aquilante, F.; Delcey, M.; Pedersen, T. B.; Galván, I. F.; Lindh, R. Inner projection techniques for the low-cost handling of two-electron integrals in quantum chemistry, *Mol. Phys.* **2017**, *115*, 2052–2064.
- [65] Freitag, L.; Knecht, S.; Angeli, C.; Reiher, M. Multireference Perturbation Theory with Cholesky Decomposition for the Density Matrix Renormalization Group, *J. Chem. Theory Comput.* **2017**, *13*, 451–459.
- [66] Győrffy, W.; Shiozaki, T.; Werner, H.-J. Analytical energy gradients for second-order multireference perturbation theory using density fitting, *J. Chem. Phys.* **2013**, *138*, 104104.
- [67] Segarra-Martí, J.; Garavelli, M.; Aquilante, F. Multiconfigurational Second-Order Perturbation Theory with Frozen Natural Orbitals Extended to the Treatment of Photochemical Problems, *J. Chem. Theory Comput.* **2015**, *11*, 3772–3784.
- [68] Guo, Y.; Sivalingam, K.; Valeev, E. F.; Neese, F. SparseMaps — A systematic infrastructure for reduced-scaling electronic structure methods. III. Linear-scaling multireference domain-based pair natural or-

- bital N-electron valence perturbation theory, *J. Chem. Phys.* **2016**, *144*, 094111.
- [69] Segarra-Martí, J.; Garavelli, M.; Aquilante, F. Converging many-body correlation energies by means of sequence extrapolation, *J. Chem. Phys.* **2018**, *148*, 034107.
- [70] Menezes, F.; Kats, D.; Werner, H.-J. Local complete active space second-order perturbation theory using pair natural orbitals (PNO-CASPT2), *J. Chem. Phys.* **2016**, *145*, 124115.
- [71] Zgid, D.; Ghosh, D.; Neuscamman, E.; Chan, G. K.-L. A study of cumulant approximations to n -electron valence multireference perturbation theory, *J. Chem. Phys.* **2009**, *130*, 194107.
- [72] Kurashige, Y.; Yanai, T. Second-order perturbation theory with a density matrix renormalization group self-consistent field reference function: Theory and application to the study of chromium dimer, *J. Chem. Phys.* **2011**, *135*, 094104.
- [73] Kurashige, Y.; Chalupský, J.; Lan, T. N.; Yanai, T. Complete active space second-order perturbation theory with cumulant approximation for extended active-space wavefunction from density matrix renormalization group, *J. Chem. Phys.* **2014**, *141*, 174111.
- [74] Sharma, S.; Chan, G. K.-L. Communication: A flexible multi-reference perturbation theory by minimizing the Hylleraas functional with matrix product states, *J. Chem. Phys.* **2014**, *141*, 111101.
- [75] Guo, S.; Watson, M. A.; Hu, W.; Sun, Q.; Chan, G. K.-L. N -Electron Valence State Perturbation Theory Based on a Density Matrix Renormalization Group Reference Function, with Applications to the Chromium Dimer and a Trimer Model of Poly(p-Phenylenevinylene), *J. Chem. Theory Comput.* **2016**, *12*, 1583–1591.
- [76] Sharma, S.; Jeanmairat, G.; Alavi, A. Quasi-degenerate perturbation theory using matrix product states, *J. Chem. Phys.* **2016**, *144*, 034103.
- [77] Roemelt, M.; Guo, S.; Chan, G. K.-L. A projected approximation to strongly contracted N -electron valence perturbation theory for DMRG wavefunctions, *J. Chem. Phys.* **2016**, *144*, 204113.
- [78] Sokolov, A. Y.; Chan, G. K.-L. A time-dependent formulation of multi-reference perturbation theory, *J. Chem. Phys.* **2016**, *144*, 064102.

- [79] Becke, A. D. Density-Functional Exchange-Energy Approximation with Correct Asymptotic Behavior, *Phys. Rev. A* **1988**, *38*, 3098–3100.
- [80] Weigend, F.; Ahlrichs, R. Balanced Basis Sets of Split Valence, Triple Zeta Valence and Quadruple Zeta Valence Quality for H to Rn: Design and Assessment of Accuracy, *Phys. Chem. Chem. Phys.* **2005**, *7*, 3297–3305.
- [81] Grimme, S.; Antony, J.; Ehrlich, S.; Krieg, H. A Consistent and Accurate Ab Initio Parametrization of Density Functional Dispersion Correction (DFT-D) for the 94 Elements H-Pu, *J. Chem. Phys.* **2010**, *132*, 154104.
- [82] Werner, H.-J. , **2018**, private communication.
- [83] Grimme, S. Improved Second-Order Møller–Plesset Perturbation Theory by Separate Scaling of Parallel- and Antiparallel-Spin Pair Correlation Energies, *J. Chem. Phys.* **2003**, *118*, 9095–9102.
- [84] Neese, F. Software Update: The ORCA Program System, Version 4.0, *WIREs Comput. Mol. Sci.* **2017**, e1327.
- [85] Weigend, F.; Köhn, A.; Hättig, C. Efficient use of the correlation consistent basis sets in resolution of the identity MP2 calculations, *J. Chem. Phys.* **2002**, *116*, 3175–3183.
- [86] Dunning, T. H. Gaussian basis sets for use in correlated molecular calculations. I. The atoms boron through neon and hydrogen, *J. Chem. Phys.* **1989**, *90*, 1007–1023.
- [87] Figgen, D.; Rauhut, G.; Dolg, M.; Stoll, H. Energy-Consistent Pseudopotentials for Group 11 and 12 Atoms: Adjustment to Multi-Configuration Dirac–Hartree–Fock Data, *Chem. Phys.* **2005**, *311*, 227–244.
- [88] Peterson, K. A.; Figgen, D.; Dolg, M.; Stoll, H. Energy-Consistent Relativistic Pseudopotentials and Correlation Consistent Basis Sets for the 4d Elements Y–Pd, *J. Chem. Phys.* **2007**, *126*, 124101.
- [89] Figgen, D.; Peterson, K. A.; Dolg, M.; Stoll, H. Energy-Consistent Pseudopotentials and Correlation Consistent Basis Sets for the 5d Elements Hf–Pt, *J. Chem. Phys.* **2009**, *130*, 164108.

- [90] Halkier, A.; Helgaker, T.; Jørgensen, P.; Klopper, W.; Koch, H.; Olsen, J.; Wilson, A. K. Basis-Set Convergence in Correlated Calculations on Ne, N₂, and H₂O, *Chem. Phys. Lett.* **1998**, *286*, 243–252.
- [91] Neese, F.; Wennmohs, F.; Hansen, A.; Becker, U. Efficient, Approximate and Parallel Hartree–Fock and Hybrid DFT Calculations. A ‘Chain-of-Spheres’ Algorithm for the Hartree–Fock Exchange, *Chem. Phys.* **2009**, *356*, 98–109.
- [92] Weigend, F. Accurate Coulomb-Fitting Basis Sets for H to Rn, *Phys. Chem. Chem. Phys.* **2006**, *8*, 1057–1065.
- [93] Vaucher, A.; Reiher, M. Steering Orbital Optimization out of Local Minima and Saddle Points Toward Lower Energy, *J. Chem. Theory Comput.* **2017**, *13*, 1219–1228.
- [94] Liakos, D. G.; Sparta, M.; Kesharwani, M. K.; Martin, J. M. L.; Neese, F. Exploring the Accuracy Limits of Local Pair Natural Orbital Coupled-Cluster Theory, *J. Chem. Theory Comput.* **2015**, *11*, 1525–1539.
- [95] Lee, C.; Yang, W.; Parr, R. G. Development of the Colle-Salvetti Correlation-Energy Formula into a Functional of the Electron Density, *Phys. Rev. B* **1988**, *37*, 785–789.
- [96] Perdew, J. P.; Burke, K.; Ernzerhof, M. Generalized Gradient Approximation Made Simple, *Phys. Rev. Lett.* **1996**, *77*, 3865–3868.
- [97] Perdew, J. P.; Burke, K.; Ernzerhof, M. Generalized Gradient Approximation Made Simple [Phys. Rev. Lett. 77, 3865 (1996)], *Phys. Rev. Lett.* **1997**, *78*, 1396–1396.
- [98] Zhao, Y.; Truhlar, D. G. The M06 Suite of Density Functionals for Main Group Thermochemistry, Thermochemical Kinetics, Noncovalent Interactions, Excited States, and Transition Elements: Two New Functionals and Systematic Testing of Four M06-Class Functionals and 12 Other Functionals, *Theor. Chem. Acc.* **2007**, *120*, 215–241.
- [99] Tao, J.; Perdew, J. P.; Staroverov, V. N.; Scuseria, G. E. Climbing the Density Functional Ladder: Nonempirical Meta–Generalized Gradient Approximation Designed for Molecules and Solids, *Phys. Rev. Lett.* **2003**, *91*, 146401.

- [100] Stephens, P. J.; Devlin, F. J.; Chabalowski, C. F.; Frisch, M. J. Ab Initio Calculation of Vibrational Absorption and Circular Dichroism Spectra Using Density Functional Force Fields, *J. Phys. Chem.* **1994**, *98*, 11623–11627.
- [101] Adamo, C.; Barone, V. Toward reliable density functional methods without adjustable parameters: The PBE0 model, *J. Chem. Phys.* **1999**, *110*, 6158–6170.
- [102] Staroverov, V. N.; Scuseria, G. E.; Tao, J.; Perdew, J. P. Comparative assessment of a new nonempirical density functional: Molecules and hydrogen-bonded complexes, *J. Chem. Phys.* **2003**, *119*, 12129–12137.
- [103] Staroverov, V. N.; Scuseria, G. E.; Tao, J.; Perdew, J. P. Erratum: "Comparative assessment of a new nonempirical density functional: Molecules and hydrogen-bonded complexes" [*J. Chem. Phys.* *119*, 12129 (2003)], *J. Chem. Phys.* **2004**, *121*, 11507–11507.
- [104] Andrae, D.; Häußermann, U.; Dolg, M.; Stoll, H.; Preuß, H. Energy-Adjusted Ab Initio Pseudopotentials for the Second and Third Row Transition Elements, *Theoret. Chim. Acta* **1990**, *77*, 123–141.
- [105] www.chemie.uni-bonn.de/pctc/mulliken-center/software/dft-d3 (accessed: 10.07.2017).
- [106] Goerigk, L.; Kruse, H.; Grimme, S. Benchmarking Density Functional Methods against the S66 and S66x8 Datasets for Non-Covalent Interactions, *ChemPhysChem* **2011**, *12*, 3421–3433.
- [107] Grimme, S.; Ehrlich, S.; Goerigk, L. Effect of the Damping Function in Dispersion Corrected Density Functional Theory, *J. Comput. Chem.* **2011**, *32*, 1456–1465.
- [108] Vydrov, O. A.; Van Voorhis, T. Nonlocal van Der Waals Density Functional: The Simpler the Better, *J. Chem. Phys.* **2010**, *133*, 244103.
- [109] Hujo, W.; Grimme, S. Performance of the van Der Waals Density Functional VV10 and (Hybrid)GGA Variants for Thermochemistry and Noncovalent Interactions, *J. Chem. Theory Comput.* **2011**, *7*, 3866–3871.
- [110] Becke, A. D.; Johnson, E. R. Exchange-Hole Dipole Moment and the Dispersion Interaction, *J. Chem. Phys.* **2005**, *122*, 154104.

- [111] Becke, A. D.; Johnson, E. R. Exchange-Hole Dipole Moment and the Dispersion Interaction: High-Order Dispersion Coefficients, *J. Chem. Phys.* **2006**, *124*, 014104.
- [112] Ángyán, J. G. On the Exchange-Hole Model of London Dispersion Forces, *J. Chem. Phys.* **2007**, *127*, 024108.
- [113] Becke, A. D.; Johnson, E. R. Exchange-Hole Dipole Moment and the Dispersion Interaction Revisited, *J. Chem. Phys.* **2007**, *127*, 154108.
- [114] Heßelmann, A. Derivation of the Dispersion Energy as an Explicit Density- and Exchange-Hole Functional, *J. Chem. Phys.* **2009**, *130*, 084104.
- [115] Steinmann, S. N.; Corminboeuf, C. A System-Dependent Density-Based Dispersion Correction, *J. Chem. Theory Comput.* **2010**, *6*, 1990–2001.
- [116] Gaussian 09, Revision A.02, Frisch, M. J.; Trucks, G. W.; Schlegel, H. B.; Scuseria, G. E.; Robb, M. A.; Cheeseman, J. R.; Scalmani, G.; Barone, V.; Petersson, G. A.; Nakatsuji, H.; Li, X.; Caricato, M.; Marenich, A.; Bloino, J.; Janesko, B. G.; Gomperts, R.; Mennucci, B.; Hratchian, H. P.; Ortiz, J. V.; Izmaylov, A. F.; Sonnenberg, J. L.; Williams-Young, D.; Ding, F.; Lipparini, F.; Egidi, F., Goings, J.; Peng, B.; Petrone, A.; Henderson, T.; Ranasinghe, D.; Zakrzewski, V. G.; Gao, J.; Rega, N.; Zheng, G.; Liang, W.; Hada, M.; Ehara, M.; Toyota, K.; Fukuda, R.; Hasegawa, J.; Ishida, M.; Nakajima, T.; Honda, Y.; Kitao, O.; Nakai, H.; Vreven, T.; Throssell, K.; Montgomery, J. A., Jr.; Peralta, J. E.; Ogliaro, F.; Bearpark, M.; Heyd, J. J.; Brothers, E.; Kudin, K. N.; Staroverov, V. N.; Keith, T.; Kobayashi, R.; Normand, J.; Raghavachari, K.; Rendell, A.; Burant, J. C.; Iyengar, S. S.; Tomasi, J.; Cossi, M.; Millam, J. M.; Klene, M.; Adamo, C.; Cammi, R.; Ochterski, J. W.; Martin, R. L.; Morokuma, K.; Farkas, O.; Foresman, J. B. and Fox, D. J. Gaussian, Inc., Wallingford CT, 2016.
- [117] www.schooner.chem.dal.ca/wiki/Postg (accessed: 10.07.2017).
- [118] Ghigo, G.; Roos, B. O.; Malmqvist, P.-Å. A Modified Definition of the Zeroth-Order Hamiltonian in Multiconfigurational Perturbation Theory (CASPT2), *Chem. Phys. Lett.* **2004**, *396*, 142–149.
- [119] Stein, C. J.; Reiher, M. Measuring Multi-Configurational Character by Orbital Entanglement, *Mol. Phys.* **2017**, *115*, 2110–2119.

- [120] Legeza, Ö.; Sólyom, J. Optimizing the Density-Matrix Renormalization Group Method Using Quantum Information Entropy, *Phys. Rev. B* **2003**, *68*, 195116.
- [121] Rissler, J.; Noack, R. M.; White, S. R. Measuring Orbital Interaction Using Quantum Information Theory, *Chem. Phys.* **2006**, *323*, 519–531.
- [122] Roos, B. O.; Lindh, R.; Malmqvist, P.-Å.; Veryazov, V.; Widmark, P.-O. New Relativistic ANO Basis Sets for Transition Metal Atoms, *J. Phys. Chem. A* **2005**, *109*, 6575–6579.
- [123] Aquilante, F.; Gagliardi, L.; Pedersen, T. B.; Lindh, R. Atomic Cholesky Decompositions: A Route to Unbiased Auxiliary Basis Sets for Density Fitting Approximation with Tunable Accuracy and Efficiency, *J. Chem. Phys.* **2009**, *130*, 154107–154107–9.
- [124] Aquilante, F.; Pedersen, T. B.; Lindh, R.; Roos, B. O.; Sánchez de Merás, A.; Koch, H. Accurate Ab Initio Density Fitting for Multiconfigurational Self-Consistent Field Methods, *J. Chem. Phys.* **2008**, *129*, 024113.
- [125] Hess, B. A. Relativistic electronic-structure calculations employing a two-component no-pair formalism with external-field projection operators, *Phys. Rev. A* **1986**, *33*, 3742–3748.
- [126] Wolf, A.; Reiher, M.; Hess, B. A. The Generalized Douglas–Kroll Transformation, *J. Chem. Phys.* **2002**, *117*, 9215–9226.
- [127] Reiher, M.; Wolf, A. Exact decoupling of the Dirac Hamiltonian. II. The generalized Douglas–Kroll–Hess transformation up to arbitrary order, *J. Chem. Phys.* **2004**, *121*, 10945–10956.
- [128] Aquilante, F. *et al.* Molcas 8: New Capabilities for Multiconfigurational Quantum Chemical Calculations across the Periodic Table, *J. Comput. Chem.* **2016**, *37*, 506–541.
- [129] Dolfi, M.; Bauer, B.; Keller, S.; Kosenkov, A.; Ewart, T.; Kantian, A.; Giamarchi, T.; Troyer, M. Matrix Product State Applications for the ALPS Project, *Comput. Phys. Commun.* **2014**, *185*, 3430–3440.
- [130] Keller, S.; Dolfi, M.; Troyer, M.; Reiher, M. An efficient matrix product operator representation of the quantum-chemical Hamiltonian, *J. Chem. Phys.* **2015**, *143*, 244118.

- [131] Keller, S.; Reiher, M. Spin-adapted matrix product states and operators, *J. Chem. Phys.* **2016**, *144*, 134101.
- [132] Knecht, S.; Hedegård, E. D.; Keller, S.; Kovyrshin, A.; Ma, Y.; Muolo, A.; Stein, C. J.; Reiher, M. New Approaches for ab initio Calculations of Molecules with Strong Electron Correlation., *CHIMIA* **2016**, *70*, 244–251.
- [133] Narancic, S.; Bach, A.; Chen, P. Simple Fitting of Energy-Resolved Reactive Cross Sections in Threshold Collision-Induced Dissociation (T-CID) Experiments, *J. Phys. Chem. A* **2007**, *111*, 7006–7013.
- [134] Hammad, L. A.; Gerdes, G.; Chen, P. Electrospray Ionization Tandem Mass Spectrometric Determination of Ligand Binding Energies in Platinum(II) Complexes, *Organometallics* **2005**, *24*, 1907–1913.
- [135] Zoicher, E.; Sigrist, R.; Chen, P. Threshold CID Investigation of Isomeric Cu(I) Azabox Complexes, *Inorg. Chem.* **2007**, *46*, 11366–11370.
- [136] Torker, S.; Merki, D.; Chen, P. Gas-Phase Thermochemistry of Ruthenium Carbene Metathesis Catalysts, *J. Am. Chem. Soc.* **2008**, *130*, 4808–4814.
- [137] Serra, D.; Moret, M.-E.; Chen, P. Transmetalation of Methyl Groups Supported by Pt^{II}–Au^I Bonds in the Gas Phase, in Silico, and in Solution, *J. Am. Chem. Soc.* **2011**, *133*, 8914–8926.
- [138] Fedorov, A.; Couzijn, E. P. A.; Nagornova, N. S.; Boyarkin, O. V.; Rizzo, T. R.; Chen, P. Structure and Bonding of Isoleptic Coinage Metal (Cu, Ag, Au) Dimethylaminonitrenes in the Gas Phase, *J. Am. Chem. Soc.* **2010**, *132*, 13789–13798.
- [139] Fedorov, A.; Batiste, L.; Couzijn, E. P. A.; Chen, P. Experimental and Theoretical Study of a Gold(I) Aminonitrene Complex in the Gas Phase, *ChemPhysChem* **2010**, *11*, 1002–1005.
- [140] Couzijn, E.; Zoicher, E.; Bach, A.; Chen, P. Gas-Phase Energetics of Reductive Elimination from a Palladium(II) N-Heterocyclic Carbene Complex, *Chem. Eur. J.* **2010**, *16*, 5408–5415.
- [141] Couzijn, E. P. A.; Kobylanskii, I. J.; Moret, M.-E.; Chen, P. Experimental Gas-Phase Thermochemistry for Alkane Reductive Elimination from Pt(IV), *Organometallics* **2014**, *33*, 2889–2897.

- [142] Reiher, M.; Neugebauer, J.; Hess, B. A. Quantum chemical calculation of Raman intensities for large molecules: The photoisomerization of $[\{\text{Fe}'\text{S}_4'(\text{PR}_3)\}_2(\text{N}_2\text{H}_2)]$ ($\text{S}_4'^{2-} = 1,2\text{-bis}(2\text{-mercaptophenylthio)ethane}(2-)$), *Z. Physik. Chem.* **2003**, *217*, 91–103.
- [143] Neugebauer, J.; Hess, B. A. Fundamental Vibrational Frequencies of Small Polyatomic Molecules from Density-Functional Calculations and Vibrational Perturbation Theory, *J. Chem. Phys.* **2003**, *118*, 7215–7225.
- [144] Reiher, M.; Brehm, G.; Schneider, S. Assignment of vibrational spectra of 1,10-phenanthroline by comparison with frequencies and Raman intensities from density functional calculations, *J. Phys. Chem. A* **2004**, *108*, 734–742.
- [145] Janssen, C. L.; Nielsen, I. M. B. New Diagnostics for Coupled-Cluster and Møller–Plesset Perturbation Theory, *Chem. Phys. Lett.* **1998**, *290*, 423–430.
- [146] Grimme, S.; Steinmetz, M. Effects of London dispersion correction in density functional theory on the structures of organic molecules in the gas phase, *Phys. Chem. Chem. Phys.* **2013**, *15*, 16031–16042.
- [147] Steinmetz, M.; Hansen, A.; Ehrlich, S.; Risthaus, T.; Grimme, S. Accurate Thermochemistry for Large Molecules with Modern Density Functionals. In *Density Functionals; Topics in Current Chemistry* Springer: Cham, 2014.
- [148] Weymuth, T.; Proppe, J.; Reiher, M. Statistical Analysis of Semiclassical Dispersion Corrections, **2018**, arXiv:1801.08580.
- [149] Hansen, A.; Bannwarth, C.; Grimme, S.; Petrović, P.; Werlé, C.; Djukic, J.-P. The Thermochemistry of London Dispersion-Driven Transition Metal Reactions: Getting the ‘Right Answer for the Right Reason’, *ChemistryOpen* **2014**, *3*, 177–189.
- [150] Paenurk, E.; Gershoni-Poranne, R.; Chen, P. Trends in Metallophilic Bonding in Pd–Zn and Pd–Cu Complexes, *Organometallics* **2017**, *36*, 4854–4863.
- [151] Carpenter, J. E.; McNary, C. P.; Furin, A.; Sweeney, A. F.; Armentrout, P. B. How Hot are Your Ions Really? A Threshold Collision-Induced Dissociation Study of Substituted Benzylpyridinium

- Thermometer Ions, *J. Am. Soc. Mass Spectrom.* **2017**, *28*, 1876–1888.
- [152] Tureček, F.; McLafferty, F. W. Non-Ergodic Behavior in Acetone-Enol Ion Dissociations, *J. Am. Chem. Soc.* **1984**, *106*, 2525–2528.
- [153] Tureček, F. N–C_α Bond Dissociation Energies and Kinetics in Amide and Peptide Radicals. Is the Dissociation a Non-Ergodic Process?, *J. Am. Chem. Soc.* **2003**, *125*, 5954–5963.
- [154] Shaffer, C. J.; Révész, Á.; Schröder, D.; Severa, L.; Teplý, F.; Zins, E.-L.; Jašíková, L.; Roithová, J. Can Hindered Intramolecular Vibrational Energy Redistribution Lead to Non-Ergodic Behavior of Medium-Sized Ion Pairs?, *Angew. Chem. Int. Ed.* **2012**, *51*, 10050–10053.
- [155] Simm, G. N.; Reiher, M. Systematic Error Estimation for Chemical Reaction Energies, *J. Chem. Theory Comput.* **2016**, *12*, 2762–2773.
- [156] Simm, G. N.; Proppe, J.; Reiher, M. Error Assessment of Computational Models in Chemistry, *CHIMIA* **2017**, *71*, 202–208.
- [157] Proppe, J.; Husch, T.; Simm, G. N.; Reiher, M. Uncertainty quantification for quantum chemical models of complex reaction networks, *Faraday Discuss.* **2017**, *195*, 497–520.